IJE TRANSACTIONS B: Applications Vol. 28, No. 2, (February 2015) 180-189

International Journal of Engineering

Journal Homepage: www.ije.ir

Frictional Strain Hardening-softening in Experimental and Numerical Investigation of Arching Effect

G. Moradi, A. R. Abbasnejad*

Department of Geotechnical Engineering, University of Tabriz, Tabriz, Iran

PAPER INFO

Paper history:
Received 09 May 2014
Received in revised form 03 October 2014
Accepted 13 November 2014

Keywords:
Arching Effect
Modified Mohr Coulomb
Frictional Hardening-softening
ABAQUS

ABSTRACT

In the current paper, the results of a numerical simulation that were verified by a well instrumented experimental procedure for studying the arching effect over a trapdoor in sand is presented. To simulate this phenomenon with continuum mechanics, the experimental procedure is modeled in ABAQUS code using stress dependent hardening in elastic state and plastic strain dependent frictional hardening-softening with Mohr Coulomb failure criterion applying user sub-routine. The apparatus comprises of concentric circular trapdoors with different diameters that can yield downward while stresses and deformations are recorded simultaneously. As the trapdoor starts to yield, the whole soil mass deforms elastically. However, after an immediate specified displacement, depending on the diameter of the trapdoor, the soil mass behaves plastically. This behavior of sand occurs due to the flow phenomenon and continues until the stress on trapdoor is minimized. Then the failure process develops in sand and the measured stress on the trapdoor shows an ascending trend. This indicates gradual separation of the yielding mass from the whole soil body. Finally, the flow process leads to establish a stable vault of sand called arching mechanism or progressive collapse of the soil body.

doi: *10.5829/idosi.ije.2015.28.02b.03*

1. INTRODUCTION

The arching phenomenon is known to engineers as the reduction of stress experienced due to yielding underground structure. Arching plays an important role in structure-soil interaction such as: excavation, retaining structures, pile group effects, tunnel boring machines, culverts and various underground facilities. The essential features of arching were demonstrated by experiments on sand with a yielding trapdoor performed by Terzaghi. The shear plane theory was subsequently proposed by him in 1943. The analysis involved studying the equilibrium horizontal element of soil, assuming that soil has perfectly plastic behavior [1]. Later, experimental modeling the soil arching as the transfer of soil pressure from a yielding support to an adjacent non-yielding support, was done by several researches such as Liam Finn [2]; Getzele et al. [3]; Ladanyi et al. [4]; Borghignoli [5]; Vardoulakis et al. [6]; Otani et al. [7]; Sadrekarimi and Abbasnejad [8].

Hosseinian and Cheraghi Seifabad [9] investigated arching effect of retained structure with anchorage method, Plaxis 3D Tunnel software was used to model fine-grain (CL-ML) with hardening soil behavior which simulates soil material. A comparison between the results gained from the 3D FE analyses and the more or less conventional method shows that the classical method is much more on the safe side. Dalvi and Pise [10] investigated arching action considering passive earth pressure in non-cohesive backfill. The backfill was assumed to move upward in a form of catenary arch due to arching. An illustrative example was solved to show the effect of the angle of major principal plane on earth pressure distribution on retaining wall considering arching for different wall friction angles and soil friction angles and applicability of proposed formulation is compared with model test results.

*Corresponding Author's Email: abbasnejad_ar@yahoo.com (A. R. Abbasnejad)

Please cite this article as: G. Moradi, A.R. Abbasnejad, Frictional Strain Hardening-Softening in Experimental and Numerical Investigation of Arching Effect, International Journal of Engineering (IJE), TRANSACTIONS B: Applications Vol. 28, No. 2, (February 2015) 180-189

Recently, the discrete element method (2D/3D DEM) has been employed to model the tunnel face failure considering arching effect (e.g. Melis Maynar and Medina Rodriguez [11]; Vardakos et al. [12]; Chen et al. [13], etc.). The coupled DEM/FEM method has also been used to investigate the earth pressure acting on the tunnel lining (the surrounding soil being modeled using DEM with the lining modeled using FEM [14]. Sadrekarimi and Abbasnejad [15, 16] used an instrumented apparatus that comprised of concentric circular trapdoors with different diameters that could yield downward while stresses and deformations were recorded simultaneously. They also compared the results with Terzaghi's theory and upper boundary solution suggested by Atkinson and Pots [17]. They also introduced an equation for the stable arch obtained from the experiment.

Modeling arching phenomenon in continuum mechanics and finding a soil model that can describe the behavior of the soil during arching especially in granular soils is the place of discussion. In spite of vast investigations on soil arching, there is not an ample study on the modeling of the arching effect considering the hardening and softening phenomenon occurred during it. Current paper presents results of a numerical and experimental work in which the best proper constitutive soil model is investigated.

2. SOIL PROPERTIES

The test soil was a cohesionless silty sand with passed percentage of 100 and 9% from sieves No. 10 and No. 200, respectively. The gradation curve coefficient of curvature (C_c) and coefficient of uniformity (C_u) were 1.1 and 5.3. The sieve test result is illustrated in Figure 1. The specific gravity of solid particles was 2.61 and the moisture content was kept at 3% throughout the experiments. The soil was classified as SP-SM according to USCS. The maximum and minimum dry densities were measured as 16.77 and 12.26 kN/m^3, respectively.

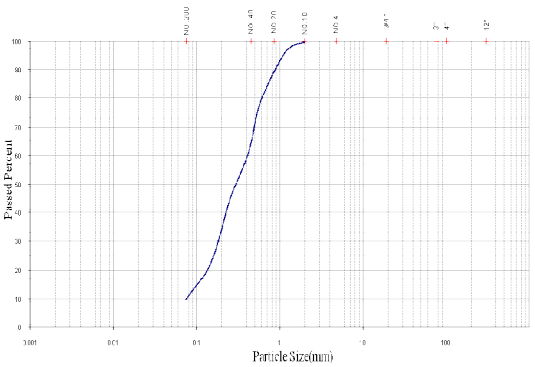

Figure 1. Sieve analysis of the test soil

3. FINITE-ELEMENT MODELING METHODOLOGY

Numerical modeling of the arching effect was performed using "ABAQUS 2012" program with modifications in stress and strain hardening-softening model. ABAQUS provides a wide range of tools like Explicit Finite-Element-Method to solve geotechnical boundary value problems with moderate to large deformations [18].

For simulating the arching effect, a 2D model with plain strain assumption is performed. Model correction in this study is done via a subroutine written in FORTRAN code and linked to ABAQUS to define the plastic strain hardening and softening behavior and also dependency of elastic modulus to the mean stress.

4. CONSTITUTIVE MODEL

In this research, we adopted Modified Mohr–Coulomb constitutive model with stress dependent stiffness during elastic strains and strain hardening-softening dependency in plastic section both in pre and post peak zones.

4. 1. Stress Dependent Elastic Modulus Pre-yield behavior is modeled as linear elastic with a secant shear modulus (G_S):

$$Gs = \frac{\tau_y}{\gamma_y} \tag{1}$$

where τ_y and γ_y are yield shear strain and stress, respectively. While γ_y can be directly measured from the test data (the shear stress that corresponds to $\delta\chi_y$), to compute γ_y, a shear zone thickness needs to be assumed. Before formation of the shear band, shear strain can be assumed to be more or less uniformly distributed throughout the whole depth, D, of the soil specimen. Hence, γ_y can be defined as:

$$\gamma_y = \frac{\delta\chi_y}{D} \tag{2}$$

The same can be applied for the peak shear strain γ_p (assuming that the shear band has not yet formed):

$$\gamma_p = \frac{\delta\chi_p}{D} \tag{3}$$

Consequently, the plastic shear strain at peak will be:

$$\gamma_p^p = \frac{\delta\chi_p - \delta\chi_y}{D} \tag{4}$$

The Young's modulus, E, was obtained from:

$$E = \frac{9KG_s}{3K + G_s} \tag{5}$$

where K is bulk modulus. Both the bulk modulus, K, and the second shear modulus, G_s, are stress dependent and in order to take this dependency into account, the model uses the following equations:

$$K = K_0(\frac{P}{P_{ref}})^b \tag{6}$$

$$G_s = G_0(\frac{P}{P_{ref}})^b \tag{7}$$

where p_{ref} is the reference pressure for which $K = K_0$ and $G_s = G_0$. The pressure exponent, b, is a model parameter expressing the variation of the elastic modules with the isotropic pressure. The value of b is reported to vary from 0.435, at very small strains, to 0.765, at very large strains according to Wroth et al. [19]. A value of 0.5 captures most of the important features of increased shear stiffness with pressure [20].

Poisson's ratio (ν) can be defined using the following equation:

$$\nu = \frac{3K - 2G_s}{2(3K + G_s)} \tag{8}$$

In this research due to changes in stress state during the analysis, the elastic modulus is defined according to the normal stress.

4. 2. Frictional Hardening Vermeer and de Borst [21] proposed Equation (9) for frictional hardening behavior of geotechnical material, in which mobilized friction angle (φ_m) depends on plastic strain (γ_p) and gradually increases to reach the peak friction angle:

$$Sin\,\varphi_m = 2(\frac{\sqrt{\gamma_p \times \gamma_p^p}}{\gamma_p + \gamma_p^p}) Sin\,\varphi_p \tag{9}$$

where, γ_p^p is shear plastic strain at peak friction angle φ_p. The equation to present the variable dilation angle put forward by Rowe [22] is called stress dilatancy equation and is as follows:

$$Sin\,\Psi_m = \frac{\sin\varphi_m - \sin\varphi_{cr}}{1 - \sin\varphi_m \sin\varphi_{cr}} \tag{10}$$

$$Sin\,\varphi_{cr} = \frac{\sin\varphi_p - \sin\Psi_p}{1 - \sin\varphi_p \sin\Psi_p} \tag{11}$$

where Ψ_m and φ_m are mobilized dilation angle and peak dilation angle, respectively. φ_{cr} is the critical friction angle or friction angle of constant volume. The mobilized dilatation angle is initially negative and increases with increase of plastic strain. To prevent this high value of negative dilation angle in small strains, following equation was presented by Soreide et al. [23], which also is used in this paper in modeling dilation behavior of sand:

$$Sin\,\Psi_m = \sin\Psi_p(\frac{\sin\varphi_m}{\sin\varphi_{cr}})^p \tag{12}$$

where, P is constant value and controls the shape of the curve. In the current paper, the changes of mobilized dilation angle is assumed to have a linear relation with mobilized friction angle and P value is considered to be 1.

4. 3. Frictional Softening After formation of the shear band (i.e. right after the peak), adopting the two-block model of shearing of Shibuya et al. [24], it is assumed that all plastic shear deformation takes place within the shear band, while the rest of the soil body remains elastic. Assuming the width of the shear band, d_B, equal to $16d_{50}$ [25], where d_{50} is the mean particle size of the sand, the plastic shear strain at which softening is completed, γ_f^p, will be:

$$\gamma_s^p = \gamma_p^p + \frac{\delta\chi_p^p - \delta\chi_y}{16d_{50}} = \frac{\delta\chi_p^p - \delta\chi_y}{D} + \frac{\delta\chi_p^p - \delta\chi_y}{16d_{50}} \tag{13}$$

Strain softening is introduced by reducing the mobilized friction angle φ_m and the mobilized dilation angle Ψ_m with the increase of plastic octahedral shear strain:

$$\varphi_m = \begin{bmatrix} \varphi_p - \frac{\varphi_p - \varphi_{res}}{\gamma_s^p}\gamma_{oct}^p & for\ \gamma_p^p \le \gamma_{oct}^p < \gamma_f^p \\ \varphi_{res} & for\ \gamma_{oct}^p > \gamma_f^p \end{bmatrix} \tag{14}$$

$$\Psi_m = \begin{bmatrix} \Psi_p(1 - \frac{\gamma_{oct}^p}{\gamma_s^p}) & for\ \gamma_p^p \le \gamma_{oct}^p < \gamma_f^p \\ \Psi_{res} & for\ \gamma_{oct}^p > \gamma_f^p \end{bmatrix} \tag{15}$$

where φ_p and φ_{cr} are peak mobilized friction angle and critical friction angle, respectively; Ψ_p is peak dilation angle; and γ_s^p is plastic octahedral shear strain at the end of softening.

4. 4. Stress Dependent Friction and Dilation Angle Due to this fact that friction and dilation angles depend upon confining pressure, which also was observed in the laboratory tests, and in order to determine shear strength parameters corresponding to the relevant stress levels, direct shear tests under various surcharges were carried out. The magnitude of the internal friction angle φ depends on the magnitude of the state of the stress for a particular soil [17]. The lower is the normal load, the higher is the φ angle. But according to the stress-dilatancy theory, the void ratio, water content and dilatancy are also important as well as shear and normal effective stresses in analyzing the results and soil behavior. The stress- dilatancy criteria

equation is given by:

$$\frac{\tau}{\sigma} = \tan(\varphi_{cr} + \Psi) \quad (16)$$

In the above equation, the angle of dilation Ψ depends on the initial state. So we modified the magnitude of the test results according to the stress-dilatancy theory. Shibuya et al. [24] have shown that the simple shear model only needs to be developed along the shear band. The relationship between the direct shear peak φ_p and residual or critical state angle of friction φ_{cr} can be approximated as:

$$\tan\varphi_p = \tan\varphi_{cr} + \alpha \tan\psi_p \quad (17)$$

where α is a constant value. With an optimum shear box apparatus (no rotation of the loading platen, smooth end walls, opening size between top and bottom platen equal to the thickness of the shear band) α can be taken equal to 1 [24]. The plane strain peak angle of friction φ_p can then be computed as [26]:

$$Sin\varphi_p = \frac{\tan\varphi_p}{\sin\Psi_p + \sin\Psi_p \tan\varphi_p} \quad (18)$$

Following the above researches, 21 simple direct shear tests are carried out on the mentioned sand. In these tests, parameters for sand in 3 different relative densities and 7 different applied normal pressures which was changed from 7 kPa to 300 kPa were studied. The results are illustrated in Figures 2 and 3. The peak internal friction angle is modified using Equation (17).

4. 5. Constitutive Model Verification To verify the capability of the modified Mohr–Coulomb constitutive model to reproduce actual soil behavior, a series of FE simulations of the direct shear test have been compared to laboratory data. Figures 4 to 9 illustrate the model calibration for dense, medium and loose (sand dry density=17, 15.5 and 12.75 kN/m^3) sand (d_{50} =0.3 mm) based on direct shear test. The initial depth of the soil sample was D=20 mm and the vertical effective stress varied from 7 to 300 kPa.

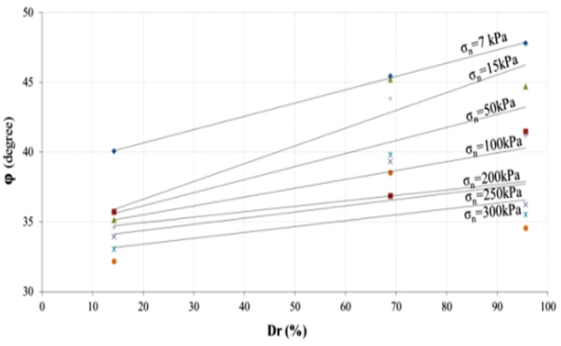

Figure 2. Internal friction angle φ against relative density

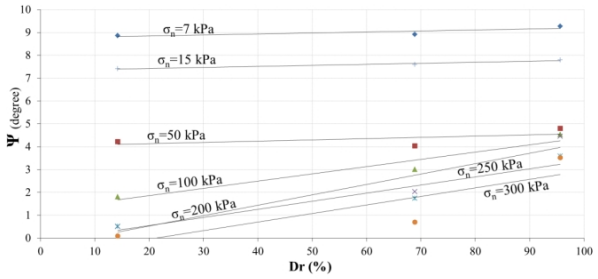

Figure 3. Dilation angle Ψ against relative density

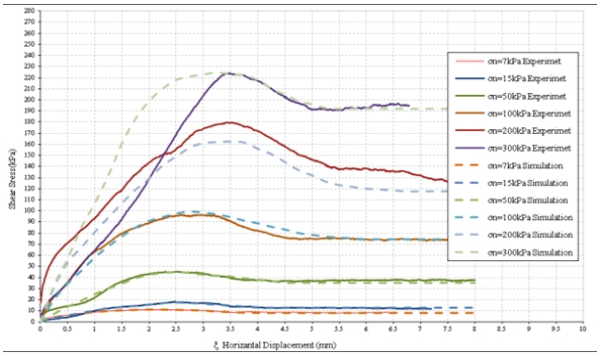

Figure 4. Comparison of the shear stress curves between laboratory direct shear tests and the results of the constitutive model for dense sand (D_r=95%)

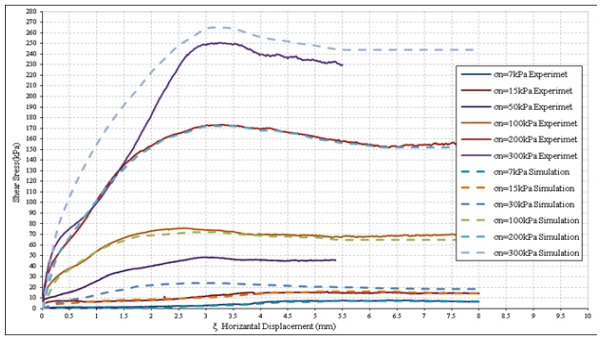

Figure 5. Comparison of the shear stress curves between laboratory direct shear tests and the results of the constitutive model for moderately dense sand (D_r=77%)

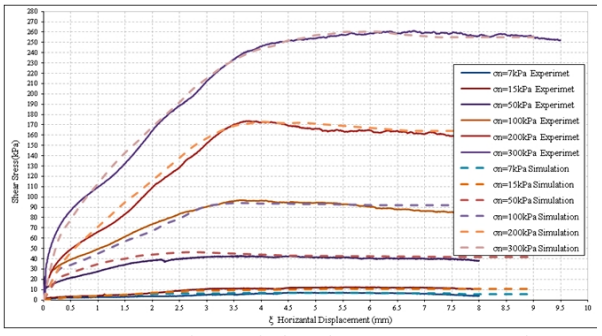

Figure 6. Comparison of the shear stress curves between laboratory direct shear tests and the results of the constitutive model for loose sand (D_r=15%)

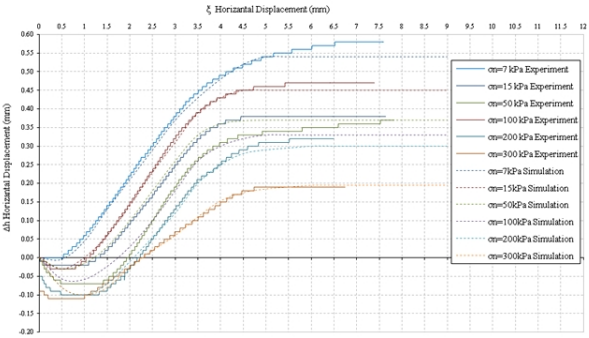

Figure 7. Comparison of the vertical dispalsements between laboratory direct shear tests and the results of the constitutive model for dense sand (D_r=95%)

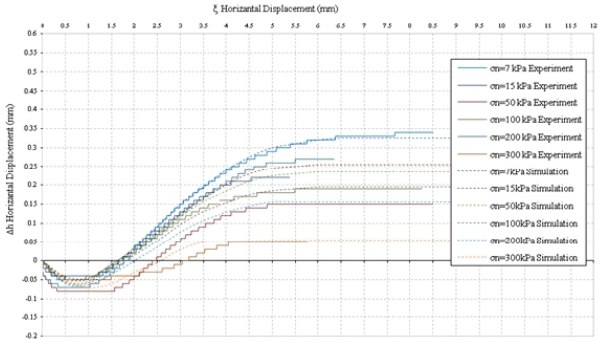

Figure 8. Comparison of the vertical dispalsements between laboratory direct shear tests and the results of the constitutive model for moderately dense sand (D_r=77%)

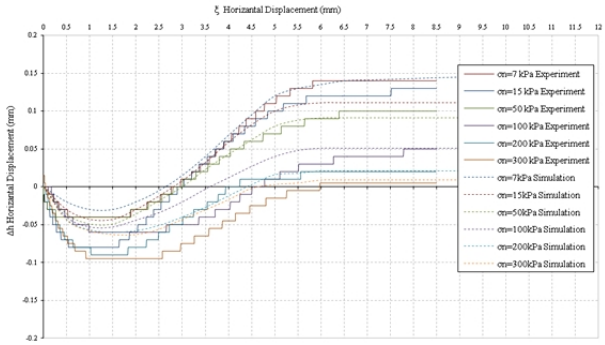

Figure 9. Comparison of the vertical dispalsements between laboratory direct shear tests and the results of the constitutive model for loose sand (D_r=15%)

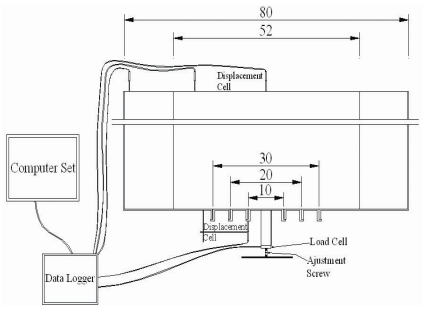

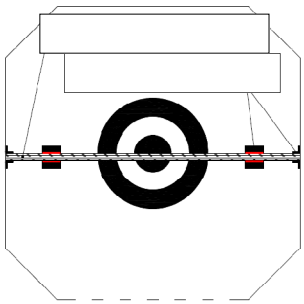

Figure 10. Schematic diagrams of the apparatus

As illustrated in Figures 4 to 9, the comparison between simulated and laboratory curves are quite satisfactory. In conclusion, despite its simplicity and (perhaps) lack of generality, the constitutive model can capture adequately the predominant mode of deformation of the specific problem studied here in a reasonable simplification to a complex soil behavior.

5. EXPERIMENTAL MODELING

5. 1. The Model Properties An apparatus was designed and constructed. The whole system is schematically shown in Figure 10. The sand container was 0.358 m^3 in volume and 60 cm in height with an octagonal horizontal cross section with a 98 cm diameter circumferential circle. The container was made of 4 mm thick steel plate strengthened with stiffeners. The container was divided into two parts using a transparent plaxy glass so that the soil could be observed by opening the side of the container. The absolute volume of the container that could be filled with sand was 0.179 m^3. Three concentric circular trapdoors were mounted under the base of the container, as shown in Figures 10 and 12. The trapdoors were 10, 20 and 30 cm in diameter which could yield downward separately by a very sophisticated computerized system as shown in Figures 10 and 11. The load magnitudes on the trapdoors, caused by the pressure of the overburden soil, were measured using a load cell. The displacement of the trapdoors and also the surface of the soil due to trapdoor yielding were monitored using Linear Variable Deferential Transformer (LVDT) installed under the platform and over the soil surface.

5. 2. Test Procedure At the beginning, without any displacement, the normal stress $\sigma_\circ$ applied to the trapdoor is γh, in which γ is the density of the sand and h is the height of the mass of the sand in the container. In order to deposit the sand in loose condition it was poured from a defined height through a sieve No. 10; and in order to produce dense sand each layer of sand

was compacted evenly with a 4.54 kg rammer. Each layer of soil was 5 cm thick, and the height of falling rammer and number of blows were varied depending on the expected densities. This stage was very time consuming and several tests were carried out to make sure that the soil density was the same throughout the whole mass. Having filled the container with sand, the nuts and bolts holding the trapdoor were unscrewed while the upward pressure on the trapdoor was being adjusted so that the trapdoor did not displace. This was a curtail point of course. At this stage the recorded stress was very close to γh. Following this stage the trapdoor was slowly yielded downward with loosening the major screw of the load cell. This trend continued until the load displayed by the load cell tended towards an asymptote.

6. RESULTS

The test results with 10, 20 and 30 cm diameter trapdoors for loose sand (D_r=14%) are depicted in Figures 13-15, as examples. For comparing, below each picture, the contours of total plastic strain obtained from numerical study are presented. Regarding the pictures the progress of the total plastic stain is same as shown in the experiments. In Figures 16-18, graphs of the σ/σ_0 (the ratio of normal stress applied on the trapdoor during any stage of yielding to the same stress at the initial state of trapdoor with no displacement) against trapdoor downward displacement (ΔH) both in experimental and numerical investigations are illustrated. The ratio σ/σ_0 defines stress reduction level due to arching effect.

Figure 11. General view of the test system

Figure 12. Ttrapdoors, load cell and displacement gauge

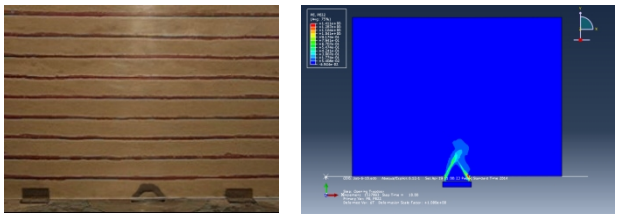

(a) Experimental results **(b)** Numerical analysis contours

Figure 13. Comparing the experimental formation of arching and plastic contours for 10 cm trapdoor diameter (D_r=14%)

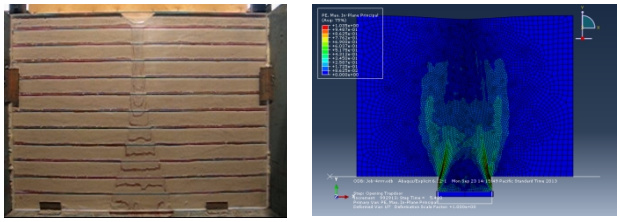

(a) Experimental results **(b)** Numerical analysis contours

Figure 14. Comparing the experimental formation of arching and plastic contours for 20 cm trapdoor diameter (D_r=14%)

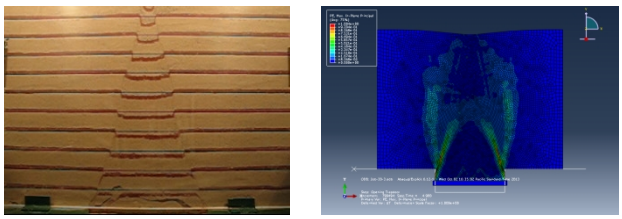

(a) Experimental results **(b)** Numerical analysis contours

Figure 15. Comparing the experimental formation of arching and plastic contours for 30 cm trapdoor diameter (D_r=14%)

7. DISCUSSION

Referring to Figures 16-18, it is observed that at the early stages of the trapdoor yielding, stress applied on the trapdoor due to soil weight decreases sharply as the trapdoor yields. At this stage, the whole mass of sand behaves mostly elastic. As the trapdoor yield proceeds, the stress ratio decreases and tends toward a minimum value, keeps on a constant level and then increases again until it tends toward an ultimate level. While a stable arch forms, the ultimate level tends to a constant value. But when an unstable arch mechanism occurs and the soil mass collapses progressively, the ultimate ratio displays increasing behavior. This behavior is true for all trapdoors. However, as the diameter of the trapdoor increases and/or the relative density of sand decreases, the minimum and ultimate stress ratios both increase. This behavior may be interpreted as follows. As the trapdoor yield starts, the overlying soil weight, exerted

by the trapdoor, is transmitted gradually onto the container base, surrounding the trapdoor. For this reason at initial stage of the trapdoor yielding, in which the sand mass behaves mostly elastic, a small yield is followed by a sharp decrease in the stress carried by the trapdoor. As the trapdoor yield proceeds, random plastic points in the sand mass deform.

At this stage stress adjustment due to trapdoor yielding is not immediate and occurs with some time lag. This is attributed to the flow phenomenon that occurs due to the plastic behavior of the yielding sand mass. Then continuing the downward displacement and as the stress ratio approaches a minimum value, failure occurs. At failure state, depending on the trapdoor diameter, relative density and the dilation angle of the sand, the failing sand mass dilates which imposes further stress on the trapdoor and continues until the failure surface developes and the yielded mass of sand is separated from the whole mass. Following this stage there is no longer any stress or mass exchange between two parts. Accordingly, the load cell displays a constant value. But when the formation and extension of the plastic points are towards the soil surface, stress applying on the trapdoor increases and progressive failure is observed in the soil mass, so that the kinematics involved during trapdoor opening break down into four distinct phases. These four phases have to be compared to the variation of the stress (σ) applied on the trapdoor with its displacement (ΔH). The failure boundaries of this area start at each edge of the trapdoor in vertical direction and then converge to axis of symmetry of the trapdoor; of course the inclination of this convergence is different depending on the sand's relative density and trapdoor diameter which results in stable or unstable arch.

In the initial state corresponding to the lowest stress applied on the trapdoor, the soil has elastic behavior. To this, first state succeeds a flow phase so that the large strains occur in soil mass without considerable change in stress level.

During this phase the plastic and failure boundaries extend to join together in the axis of symmetry of the trapdoor to produce a stable arch or extend to the top of the soil mass for unstable arch. In this phase, the extension of the plastic strain causes softening in the plastic zone of the soil mass while the inner part of the soil remains elastic and due to the increase in stress level in the adjacent parts with lower elastic and plastic strains, hardening phenomenon emerges. At the end of second phase, a transitional state is started.

During this transition, total failure and separation in the two parts of the soil occurs. But in the stable arch this state leads to a constant trend of a stress level that indicates the fixed soil mass separated from the dome. But in the unstable arch, increment in stress level continues because of the progressive failure in soil mass.

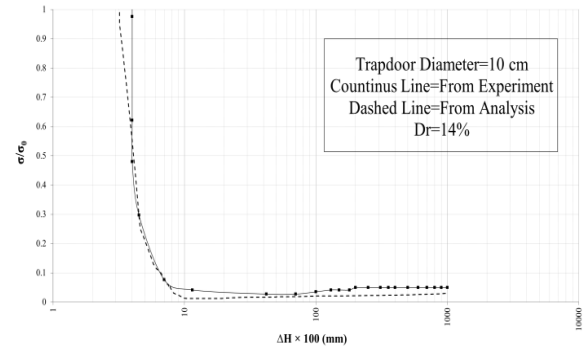

(a) D_r=14%

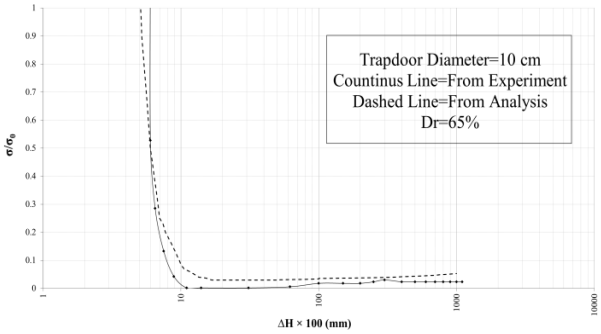

(b) D_r=65%

Figure 16. Stress ratio-yield plots for 10 cm trapdoor diameter (D_r=14% and 65%)

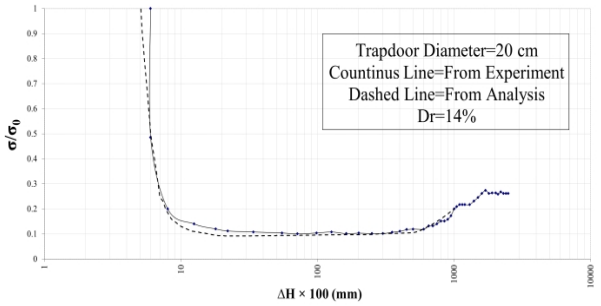

(a) D_r=14%

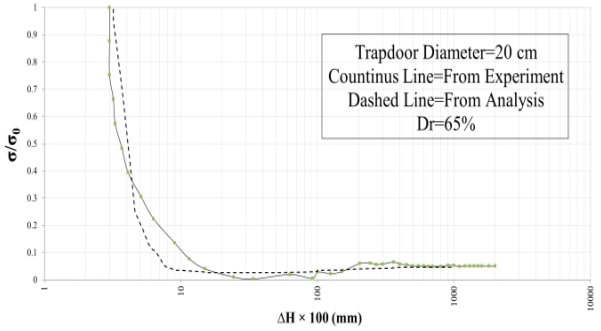

(b) D_r=65%

Figure 17. Stress ratio-yield plots for 20 cm trapdoor diameter (D_r=14.5% and 65%)

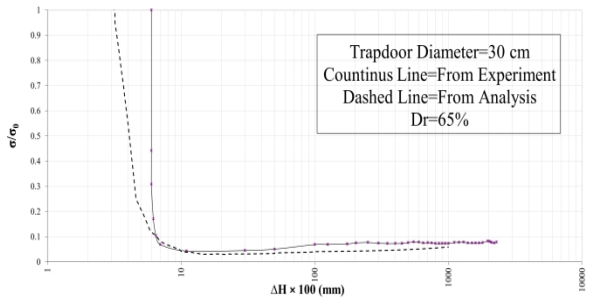

(a) Dr=14%

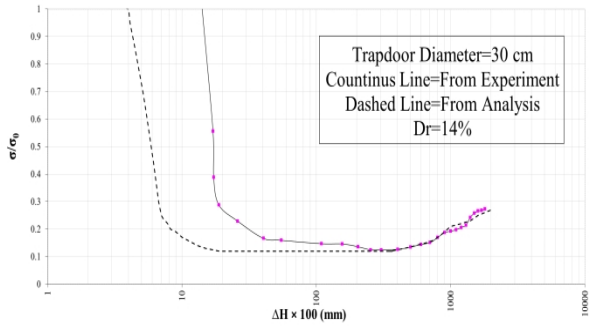

(b) Dr=65%

Figure 18. Stress ratio-yield plots for 30 cm trapdoor diameter (D_r=14.5% and 65%)

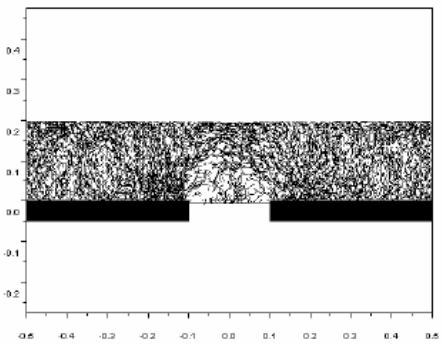

Figure 19. Model of Distinct Element Method (DEM) by Chevalier et al. [27]

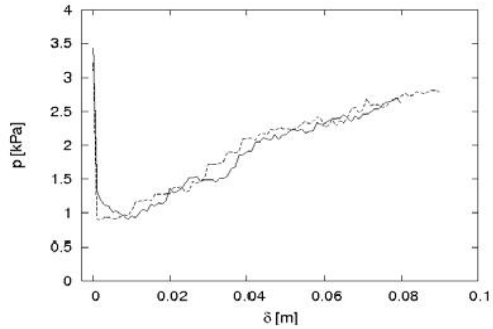

Figure 20. DEM analysis results of the trap-door tests: stress (p) versus yield (δ) plots

8. COMPARING WITH DEM METHOD

To compare the results with Distinct Element Method (DEM) predictions, the model of Chevalier et al. [27] was selected. The gradation of the sand that they used is similar to that in this research. In Figure 19, the model that they used and in Figure 20, one of the results of DEM analysis from the research of Chevalier et al. [27] are illustrated as an instance. As shown in Figure 20, only three phases could be defined and the flow phase is not taken into consideration in researches of Chevalier et al. [27]. In the finite element method which is used in this research flow phase is considered and seen in the results.

9. CONCLUSIONS

- Relative density of the soil and the trapdoor diameter, both are dominant factors affecting formation of a stable arch. As the trapdoor yields, following a small initial mostly elastic strain, the soil mass deforms plastically with larger strain rates and pressure applied onto the trapdoor decreases to a minimum value. Then, as the trapdoor yield continues, depending on the dilation angle and relative density of sand, stress level on the trapdoor increases gently and finally tends towards a constant value. At this stage, the yielding sand mass separates from the whole mass.
- Referring to the experimental and numerical investigations, there are 4 phases in arching mechanism.
- The first phase occurs immediately after a small downward displacement of the trapdoor that leads to a minimum pressure applied to the trapdoor. During this stage soil mass behaves elastically.
- The second phase starts after the pressure on the trapdoor reaches a minimum value. This phase continues in a large period of plastic strains. In this state plastic strain and failure start at each edge of the trapdoor in vertical direction and then converge to axis of symmetry of the trapdoor, of course the inclination of this extension depends on the relative density of sand and trapdoor diameter which results in stable or unstable arch. At the second stage, flow phenomenon occurs in soil mass so that considering large strains in soil mass there is no considerable change in stress level.
- The third phase starts with an increment in stress applied on the trapdoor. The separation and establishment of a stable arch occurs at this stage. In the unstable arch manner, increment continues and the stress curve does not change its behavior to transfer to the fourth state.

- The fourth phase happens in stable arch manner so that stress ratio leads to a constant value. This indicates that the separation of stable arch is completed and trapdoor bears the whole weight of the separated arch mass.
- In modeling the arching effect, the stress hardening in elastic strains and plastic strain hardening-softening behavior with Modified Mohr-Coulomb failure criterion can be used to model the realistic behavior of the sand especially flow phenomenon.
- The results of the research of Chevalier et al. [27] in which DEM was used prove that in this method the flow phase is not considerable. While in this research all phases of arching phenomenon including flow phase are possible to be modelled.

10. REFERENCES

1. Terzaghi, K., "Theoretical soil mechanics", (1943).
2. Finn, W., "Boundary value problems of soil mechanics", ***Journal of Soil Mechanics and Foundation Division, ASCE***, Vol. 89, (1963), 39-72.
3. Getzler, Z., Komornik, A. and Mazurik, A., "Model study on arching above buried structures", ***Journal of Soil Mechanics & Foundations Div***, (1968).
4. Ladanyi, B. and Hoyaux, B., "A study of the trap-door problem in a granular mass", ***Canadian Geotechnical Journal***, Vol. 6, No. 1, (1969), 1-14.
5. Burghignoli, A., "Soil interactin in buried structures", Source: Proceeding of the International Conference on Soil, (Univ of Rome, Italy), Vol. 2, (1981), 69-74.
6. Vardoulakis, I., Graf, B. and Gudehus, G., "Trap-door problem with dry sand: A statical approach based upon model test kinematics", ***International Journal for Numerical and Analytical Methods in Geomechanics***, Vol. 5, No. 1, (1981), 57-78.
7. Chevalier, B. and Otani, J., "3-d arching effect in the trap-door problem: A comparison between X-Ray ct scanning and DEM analysis", in GeoFlorida 2010@ sAdvances in Analysis, Modeling & Design, ASCE, (2010), 570-579.
8. Sadrekarimi, J. and Abbasnejad, A., "Arching effect in fine sand due to base yielding", ***Canadian Geotechnical Journal***, Vol. 47, No. 3, (2010), 366-374.
9. Hosseinian, S. and Seifabad, M.C., "Optimization the distance between piles in supporting structure using soil arching effect", ***Optimization***, Vol. 3, No. 6, (2013), 386-391.
10. Dalvi, R.S. and Pise, P.J., "Analysis of arching in soil-passive state", ***Indian Geotechnical Journal***, Vol. 42, No. 2, (2012), 106-112.
11. Maynar, M.J. and Rodríguez, L.E., "Discrete numerical model for analysis of earth pressure balance tunnel excavation", ***Journal of Geotechnical and Geoenvironmental Engineering***, Vol. 131, No. 10, (2005), 1234-1242.
12. Vardakos, S.S., Gutierrez, M.S. and Barton, N.R., "Back-analysis of shimizu tunnel No. 3 by distinct element modeling", ***Tunnelling and Underground Space Technology***, Vol. 22, No. 4, (2007), 401-413.
13. Chen, R., Tang, L., Ling, D. and Chen, Y., "Face stability analysis of shallow shield tunnels in dry sandy ground using the discrete element method", ***Computers and Geotechnics***, Vol. 38, No. 2, (2011), 187-195.
14. Dang, H.K. and Meguid, M.A., "An efficient finite–discrete element method for quasi-static nonlinear soil–structure interaction problems", ***International Journal for Numerical and Analytical Methods in Geomechanics***, Vol. 37, No. 2, (2013), 130-149.
15. Sadrekarimi, J. and Abbasnejad, A., "An experimental investigation into the arching effect in fine sand", ***International Journal of Engineering-Transactions B: Applications***, Vol. 21, No. 4, (2008), 345-360..
16. Sardrekarimi, J., Moradi, G. and Abbasnejad, A.R., "Studying and comparing the experimental and numerical investigation on to the arching effect in fine sand using plaxis code and mohr-coulomb criteria", Proceeding of 4th International conference on geotechnical engineering, Tehran, Iran, (2010).
17. Atkinson, J. and Potts, D., "Stability of a shallow circular tunnel in cohesionless soil", ***Geotechnique***, Vol. 27, No. 2, (1977), 203-215.
18. ABAQUS, " Inc. Abaqus v.6.12.1 user's manual", (2012).
19. Wroth, C., "Correlations of some engineering properties of soils", in Proceedings of the Second International Conference on the Behaviour of Off-Shore Structures, held at Imperial College, London, England. Vol., No. Issue, (1979).
20. Wroth, C., "Soil mechanics-property characterization and analysis procedures", Proceedings of the 11th International Conference on Soil Mechanics and Foundation Engineering, San Francisco, Vol. 1, (1985), 1-55.
21. Vermeer, P.A. and De Borst, R., "Non-associated plasticity for soils, concrete and rock", (1984).
22. Rowe, P., "Stress-dilatancy, earth pressures, and slopes", ***ASCE, JSMFE***, Vol. 89, (1963), 37-62.
23. Soreide, O., Nordal, S., Bonnier, P. and Mestat, P., "An implicit friction hardening model for soil materials", in Proc. 5th Europ. Conf. on Numerical Methods in Geotechnical Engng (NUMGE), Mestat (ed.), Paris, France. Presses de l'ENPC/LCPC, (2002), 155-161.
24. Shibuya, S., Mitachi, T. and Tamate, S., "Interpretation of direct shear box testing of sands as quasi-simple shear", ***Geotechnique***, Vol. 47, No. 4, (1997), 769-790.
25. Vardoulakis, I. and Graf, B., "Calibration of constitutive models for granular materials using data from biaxial experiments", ***Geotechnique***, Vol. 35, No. 3, (1985), 299-317.
26. Jewell, R. and Wroth, C., "Direct shear tests on reinforced sand", ***Geotechnique***, Vol. 37, No. 1, (1987), 53-68.
27. Chevalier, B., Combe, G. and Villard, P., "Experimental and numerical studies of load transfers and arching effect", The 12th International Conference of International Association for Computer Methods and Advances in Geomechanics (IACMAG), Goa, India, Citeseer, (2008), 273-280.

Frictional Strain Hardening-softening in Experimental and Numerical Investigation of Arching Effect

G. Moradi, A.R. Abbasnejad

Department of Geotechnical Engineering, University of Tabriz, Tabriz, Iran.

P A P E R I N F O

Paper history:
Received 09 May 2014
Received in revised form 03 October 2014
Accepted 13 November 2014

Keywords:
Arching Effect
Modified Mohr Coulomb
Frictional Hardening-softening
ABAQUS

چکیده

در این مقاله نتایج شبیه سازی عددی با نتایج حاصل از مدل آزمایشگاهی جهت بررسی پدیده قوس در ماسه ارائه شده است. روش آزمایشگاهی دقیقاً در نرم افزار ABAQUS مدل سازی گردیده و از رفتار سخت شدگی وابسته به تنش در قسمت الاستیک و همچنین سخت شدگی و نرم شدگی وابسته به کرنش پلاستیک همراه با معیار گیسختگی موهر- کولمب استفاده شده است. این رفتار توسط زیربرنامه دیگری در نرم افزار تعریف گردید. در مدل فیزیکی از دریچه های دایروی با اقطار مختلف و با قابلیت حرکت به سمت پایین همراه با ابزاربندی جهت قرائت تنش ها و جابجایی ها بهره گرفته شده است. زمانی که دریچه شروع به پایین آمدن می‌کند،توده خاک بالای دریچه در محدوده الاستیک جابه‌جا می‌شود. سپس، بعد از یک جابه‌جایی مشخص، که مقدار آن بستگی به قطر دریچه و دانسیته نسبی ماسه دارد، توده رفتار پلاستیک از خود نشان می‌دهد. این رفتار ماسه، که بدلیل بروز پدیده جریان به وقوع می‌پیوندد، تا آنجا که تنش روی دریچه کمترین شود، ادامه می‌یابد، تا این که گسیختگی در توده به وقوع می‌پیوندد و تنش اندازه‌گیری شده روی دریچه به سمت یک مقدار معین میل می‌کند. این مرحله جدا شدگی قسمتی از توده از ماسه مجاور می‌باشد و یا گسیختگی پیش رونده تا سطح ماسه ادامه پیدا می کند که منجر به افزایش تنش اعمال شده به دریچه می شود.

***doi**: 10.5829/idosi.ije.2015.28.02b.03*